Biochemistry and Biophysics Reports 35 (2023) 101513

Contents lists available at ScienceDirect

Biochemistry and Biophysics Reports

journal homepage: www.elsevier.com/locate/bbrep

The effect of histone deacetylase inhibitors on the efficiency of the CRISPR/Cas9 system

Ymer Björnson [1], Codey Y. Huang [1], Jaedyn L. Rollins [2], Guadalupe Castañeda [2], Navneet Kaur [2], Emiko Yamamoto [2], Jennifer M. Johnston [*]

1 Washington Square, Department of Biological Sciences, San José State University, San José, CA, 95112, USA

ARTICLE INFO

Keywords:
CRISPR
Gene editing
Histone deacetylase inhibitors
Valproic acid
Sodium butyrate

ABSTRACT

The CRISPR/Cas9 technology is a prominent genome-editing tool capable of producing a double-strand break in the genome. However, the modification of hematopoietic stem cells via the homology-directed repair pathway is still inefficient. Therefore, we hypothesize that histone deacetylase inhibitors, such as valproic acid (VPA) and sodium butyrate (NaB), could enhance HDR efficiency by increasing the accessibility of the genome-editing machinery. To address the potential utilization of HDAC inhibitors therapeutically, we began by assessing the effect of VPA and NaB on two cell lines representative of the two hematopoietic stem cell lineages. No statistically significant effect on cell growth or viability was observed at concentrations as high as 5 mM. At a concentration as low as 0.005 mM NaB, an enhancement in CRISPR cutting efficiency was evidenced in both cell lines. This enhancement did not appear to be locus-specific. However, an enhancement in cutting efficiency following VPA treatment does appear to be. HDR efficiency was enhanced greater than two-fold with the use of 0.005 mM VPA. These results are promising and suggest the consideration of treatment with an HDAC inhibitor in CRISPR/Cas9 genome editing protocols.

1. Introduction

CRISPR/Cas9 (Clustered Regularly Interspaced Short Palindromic Repeats) has emerged as a safe and effective way to make precise changes to the genome. CRISPR/Cas9 is an enzyme that creates a double-strand break (DSB) at a pre-selected locus [1]. There are two competing pathways that endogenously repair a DSB: (1) non-homologous end joining (NHEJ) and (2) homology-directed repair (HDR). NHEJ is error-prone and often introduces short insertions and deletions (INDELS) at the cut site, making it useful for disrupting the function of or "knocking out" a gene [2]. HDR uses an existing DNA template to repair the DSB or a previously designed DNA sequence that contains the desired modifications referred to as a donor DNA repair template. The cell will use this donor DNA repair template to correct the CRISPR/Cas9-induced DSB, resulting in the insertion of the exogenous sequence into the genome.

Primitive cells that have not yet committed to differentiation, such as hematopoietic stem cells (HSCs), are less capable of performing HDR than their progenitors [3]. Additionally, primitive HSCs exhibit delayed DSB repair compared to progenitor populations [4]. HSCs are of interest for therapeutic gene editing purposes. This cellular target is an attractive option because of the ability of HSCs to differentiate, to self-renew, and to be readily isolated, manipulated, and transplanted. However, the low editing efficiency of $CD34^{+}$ hematopoietic stem and progenitor cells (HSPCs) has historically resulted in time-consuming screening processes to sort and identify the few successfully edited cells that remain [5]. HDR efficiency in these cells following double-stranded breaks from CRISPR/Cas9 has been observed to be between 0.5 and 20%, while NHEJ was found to reach up to 100% [6]. Furthermore, quiescent and proliferating HSCs have been noted to use different repair pathways. It was demonstrated that quiescent HSCs are essentially forced to follow the NHEJ pathway because of how much time is allocated to their quiescent cell cycle [7]. Therefore, in order to make therapeutic gene editing of HSPCs worthwhile, efficient editing of primitive HSCs must be established.

To date, some of the most promising approaches have utilized small

* Corresponding author.
E-mail address: jennifer.johnston@sjsu.edu (J.M. Johnston).
[1] These authors contributed equally to this work.
[2] These authors also contributed equally to this work.

https://doi.org/10.1016/j.bbrep.2023.101513
Received 8 January 2023; Received in revised form 6 July 2023; Accepted 10 July 2023

molecules. Small molecules have been successfully implemented to either directly suppress NHEJ activity or to directly enhance HDR activity [6,8–11]. However, an alternative approach could use small molecules to inhibit the deacetylation of histones and promote a more open chromatin structure, improving accessibility to the Cas9 nuclease [12]. We hypothesized that the condensed chromatin structure restricts the CRISPR/Cas9 enzyme from accessing genomic DNA, making it difficult to produce DSBs.

Two histone deacetylase inhibitors (HDACi), valproic acid (VPA) and sodium butyrate (NaB), were assessed for the ability to enhance CRISPR/Cas 9 gene editing. We first sought to determine how representative cells of both HSC lineages respond to treatment with VPA and NaB. The CRISPR/Cas9 cutting efficiency and HDR editing efficiency were then evaluated following treatment in these cell lines.

2. Materials and methods

2.1. Chemicals and reagents

Five grams of NaB salt (Alfa Aesar #A11079-06) was dissolved in cell culture water (Lonza #17-724Q) and aliquoted into 1 mL portions for a final storage concentration of 0.91 M. Ten grams of VPA (Sigma Aldrich #P4543-10G) was dissolved in 25 ml of cell culture water (Lonza) for a final storage concentration of 1.2 M and distributed into 1 ml aliquots. Aliquots of both VPA and NaB were kept at −20° Celsius until cell treatment.

2.2. Plasmids

The pX330 plasmid for Cas9 and guide RNA expression was acquired from Addgene [13]. The pMAX plasmid for GFP expression was acquired from Lonza. Guide DNA sequences were synthesized by Integrated DNA Technologies (Newark, NJ) and phosphorylated using PNK (New England Biolabs #M0201L). They were then ligated into a BbsI (New England Biolabs #R0539L) digested pX330 plasmid using T4 DNA Ligase (New England Biolabs #M0202L). Guide integration was confirmed by sequencing.

Plasmids containing guide RNA sequences were chemically transformed into DH5α *E. coli* cells (ThermoFisher #18265017) and grown in LB broth (ThermoFisher #12780052) supplemented with ampicillin (ThermoFisher #) for a final concentration of 100 μg/ml. Large cultures were harvested and plasmid DNA was extracted using the endotoxin-free plasmid Maxi kit (QIAGEN #12362).

A donor DNA repair template containing a proof-of-principle, an exogenous fluorescent gene(green fluorescent protein, GFP) was constructed to be homologous to the *RhD* locus. Using a plasmid vector from the pCR™-Blunt II-TOPO® kit (Invitrogen, Carlsbad CA), the GFP gene and a bovine growth hormone polyA sequence were ligated respectively into the vector with arms of homology of approximately 500bp of the human *RhD* target site. This plasmid was transformed and harvested in the same manner as the guide RNAs.

2.3. Cell culture

Both human myelogenous leukemia K562 cells (ATCC #CCL-243) and human T lymphocyte Jurkat cells (ATCC #TIB-152) were cultured with 0.22 μM sterile filtered RPMI 1640 (ThermoFisher #21870076) supplemented with 10% FBS (Sigma Aldrich #F2442-500 ML) and 1% Penicillin/Streptomycin (ThermoFisher #15140163). Cells were maintained in a 37 °C incubator in a 5% CO_2 atmosphere. Cell culture media was supplemented approx. every 3 days for the purpose of maintaining healthy cell populations of at least 300,000 cells/ml to a maximum threshold of 1×10^6 cells/ml. Of note, during growth curve analysis experiments, no supplemental media was added to cell populations post-HDACi treatment. Cells for growth curve analysis were cultured using T25 flasks and populations were counted every 24 h. For the purpose of analyzing HDACi effect on CRISPR/Cas9 cutting efficiently, cells were pretreated in media with 0.005 mM NaB or VPA for 24 h prior to nucleofection. Post nucleofection, cells were cultured in six-well plates. Seventy-two hours later cells were harvested by centrifugation at 500*g* for 5 min.

2.4. Nucleofection

Electroporation was performed using either a BioRad GenePulser Xcell Electroporation (#1652660) or a Lonza Amaxa 4D Nucleofector (Lonza #AAF-1002B) with the corresponding X unit (Lonza #AAF-1002X). 1×10^6 cells were resuspended in 100 μL of Nucleofection Solution (Lonza) along with 2 μg of guide DNA (pX330 expression plasmid containing a single guide RNA) or 1 μg of pMAX. pMAX was utilized as a nucleofection control containing a sequence for a green fluorescent protein (GFP). Cells were placed in cuvettes with a gap width of 0.4 cm as recommended by the manufacturers for mammalian cells. BioRad cuvettes (BioRad #1652081) were used with the BioRad GenePulser and Lonza cuvettes were used with the Amaxa 4D Nucleofector (Lonza #V4XC-2012). The K562 and Jurkat nucleofection presets were used to deliver the electrical pulse. Successful delivery of plasmid DNA was assessed by analyzing the positive control containing pMAX via flow cytometry 72 h after nucleofection.

2.5. Flow cytometry

Cell viability and cell growth were analyzed using an Attune NxT flow cytometer (Invitrogen). The Attune Focusing fluid (Invitrogen #4488621), Attune wash, and shutdown fluid (Invitrogen #A24974, #A24975) were used per the manufacturer's recommendation. GFP analysis was also done using the Attune NxT flow cytometer and analyzed using the Attune NxT software (Invitrogen) to confirm successful electroporation.

2.6. DNA extraction and amplification

Seventy-two hours after electroporation, genomic DNA was isolated using the Qiagen DNEasy Blood & Tissue kits (Qiagen #69504). The region surrounding the target site was PCR amplified using the following primers for TIDE analysis.

RhD forward primer 5′ AACTGAGCACAGCAGGAA
RhD reverse primer 5′ GCCCAGGCTGCTTCTAAAGG
vWF forward primer 5′ GCACTGCACCAATGGCTCTG
vWF reverse primer 5′ CGGTACACTGTTGTTATCATAG

To confirm targeting of GFP to the *RhD* locus, the following primers were used. Of note, the forward primer annealed outside of the 5' region of homology included in the donor DNA repair template.

Forward primer 5′ TCACCCTAAGGCTGGATCAGG
Reverse primer 5′ ATGTTGCCGTCCTCCTTGAAGTCG

PCR reactions were verified to be successful by running 5 μL on a 1% Agarose gel. The remaining 20 μL was sent to McLab (South San Francisco, CA) for PCR cleanup and sequencing.

2.7. Measurement of allele modification using TIDE

The online Tracking of INDELS by Decomposition (TIDE) software was utilized to analyze allele modification frequencies. Specifically, the algorithm-based software detects INDELS in the amplified DNA via input of two raw sequencing files: (1) a control file and (2) a test sample file. The control sequence data files used for reference were sequences obtained from untreated K562 or Jurkat negative control cells. The test sample sequence data files used were sequences obtained from the

drugged K562 or Jurkat cells. The guide RNA sequence was input as a character string. Default parameters were used. The decomposition window was set so as to cover the largest possible window of high-quality traces. The TIDE software then determined the frequency of breaks at the guide RNA sequence site as previously described [14]. The number of breaks was compared between untreated and drugged hematopoietic cells. The software is available at https://tide.nki.nl/

2.8. Statistical analysis

Results are displayed as the mean ± standard deviation. For the comparison of two groups an unpaired student *T-test* was performed using the Graphpad PRISM software. Data was then compiled into figures and exported. A value of $p < 0.05$ was considered statistically significant.

3. Results

3.1. HDACi at lower concentrations do not affect the growth potential of hematopoietic cell lines

The effect of both VPA and NaB was assessed on the growth pattern of two hematopoietic cell lines representative of the two lineages derived from the HSC. Cells from the myeloid erythroid leukemic K562 cell line and the immortalized T lymphocyte Jurkat cell line were treated with HDACi concentrations ranging from 500 mM to 0.5 μM (Fig. 1A). It is important to note that after initial washing, no fresh media was applied to the cells in order to assess proliferation as a result of cell division. Thus, cell proliferation was not a continuous process.

As expected, K562 cells treated with VPA displayed a dose-response relationship (Fig. 1B). K562 cells at the two highest concentrations tested (300 mM and 100 mM) did not proliferate while those treated at lower concentrations did. No statistical significance was noted between the growth of untreated K562 cells and the 50 mM ($p = 0.3782$), 5 mM ($p = 0.7993$), 0.5 mM ($p = 0.9934$), 0.05 mM ($p = 0.9987$), 0.005 mM ($p = 0.9956$), 0.0005 mM ($p = 0.9987$), and 0.0005 mM ($p = 0.9462$) VPA treated K562 cells. In addition, a significant decrease in cell growth and viability (S1 Fig) was not observed between the untreated cells and the concentrations as high as 0.5 mM VPA. A similar response was observed with K562 cells treated with NaB (Fig. 1C). At the highest dose (500 mM), cell proliferation was not evident and viability was affected ($p = 0.0001$) (S1 Fig). However, at lower doses of NaB, no statistically significant difference in growth was observed between the untreated cells and K562 myeloid cells treated with 5 mm ($p = 0.0693$), 0.5 mM ($p = 0.8985$), 0.05 mM ($p = 0.6209$), and 0.005 mM ($p = 0.9151$). NaB-treated K562 cells appeared to display similar growth curves. In addition, no change in morphology was observed (data not shown). Thus, we can conclude the proliferation of K562 cells is not significantly affected following the addition of either VPA or NaB.

In the same manner, a dose-response curve was evident in Jurkat cells treated with both VPA and NaB. However, Jurkat cells appear to be more susceptible to VPA and NaB. For example, Jurkat cells treated with VPA at 300 mM ($p < 0.0001$), 100 mM ($p = 0.0002$), and 50 mM ($p = 0.0008$) were observed to proliferate at a significantly different rate than untreated cells (Fig. 1D). However, a significant difference was not observed between untreated Jurkat cells and Jurkat cells treated with 5 mM ($p = 0.2312$), 0.5 mM ($p = 0.8451$), 0.05 mM ($p = 0.8645$), 0.005 mM ($p = 0.9465$), and 0.0005 mM ($p = 0.8208$) VPA. A similar trend was observed with Jurkat cells treated with NaB (Fig. 1E). Jurkat cells treated with 50 mM NaB ($p = 0.0008$) were observed to proliferate at a significantly slower rate compared to untreated cells. However, this was not the case with Jurkat cells treated with lower NaB concentrations. A significant difference in growth was not observed between the untreated cells and the 5 mM ($p = 0.2312$), 0.5 mM ($p = 0.8451$), 0.05 mM ($p = 0.8645$), 0.005 mM ($p = 0.9465$), and 0.0005 mM ($p = 0.8208$) NaB treated cells. In addition, no effect on viability was evidenced upon treatment of Jurkat cells with these lower doses of VPA and NaB (S2 Fig). Therefore, concentrations of HDACi lower than 5 mM should be tolerated in HSPCs. Thus, we chose to utilize a HDACi concentration of 0.005 mM for our subsequent analyses.

3.2. HDACi enhance the ability of RhD CRISPR guide RNAs to produce a double-strand break

The *RhD* locus encodes for the D blood antigen located on the surface of red blood cells and is used to clinically classify individuals as having either an Rh-positive or Rh-negative blood type. In K562 cells, the RhD protein is found to be minimally expressed (proteinatlas.org) [15,16]. Therefore, several guide RNAs specific to the *RhD* locus near the start codon were evaluated for cutting efficiency in K562 cells following treatment with an HDACi (Fig. 2A). Both HDACi treated and untreated K562 cells were then nucleofected with a Cas9 expression plasmid containing one of the RhD guide RNAs (Fig. 2B). Cells were then incubated for 72 h to allow cleavage at the guide recognition site. Genomic DNA was then isolated from both guide RNA-treated cells and naive untreated cells (negative control). DNA sequences of HDACi-treated cells were aligned to that of the DNA from the naive negative control cells to scan for the presence of INDELs at the target site (S2 Fig A). An algorithm-based software known as TIDE was used to validate each guide RNA's ability to induce DSBs at their predicted cleavage site (S2 and S3 Fig) [15].

Overall, a greater cutting efficiency was observed among the RhD guide RNAs in K562 cells following treatment with VPA (Fig. 2C). Specifically, a significant enhancement was observed with the −11 ($p = 0.0348$), −18 ($p = 0.0006$), and +58 ($p < 0.0001$). A similar though nonsignificant trend was observed with the +18 RhD ($p = 0.0985$) guide RNAs. Similarly, pretreatment with NaB yielded greater cutting efficiencies among all of the RhD guide RNAs tested (Fig. 2D). A significant enhancement was observed with the −33 ($p < 0.0001$), −18 ($p < 0.0001$), +18 ($p < 0.0001$), +19 ($p < 0.0001$), and +58 ($p = 0.0258$) RhD guide RNAs. The cutting efficiency of the CRISPR RhD guide RNAs was enhanced overall.

3.3. HDACi enhance the ability of vWF CRISPR guide RNAs to produce a double-strand break

The effect of HDACi on the cutting efficiency of CRISPR guide RNAs was evaluated at a second locus, the *von Willebrand Factor* (*vWF*) locus. As opposed to the *RhD* locus, the *vWF* locus is not found to be expressed in K562 cells [15,16]. Six different RNAs spanning the stop codon of the *vWF* gene were evaluated for cutting efficiency (Fig. 3A). Using the same experimental design as noted above (Fig. 2B), both HDACi treated and untreated hematopoietic cells were nucleofected with a Cas9 expression plasmid containing one of the depicted guide RNAs. The presence of INDELS was identified and used to quantify cutting efficiencies of the guide RNAs using the TIDE software [14]. In K562 cells, upon treatment with either VPA or NaB, a statistically significant difference is not readily apparent in the cutting efficiency of the vWF guide RNAs (Fig. 3B and C). The cutting efficiency of only one vWF guide RNA (+39) was found to be enhanced ($p = 0.162$) upon treatment with NaB. A similar result was noted in a second hematopoietic cell line (Jurkat cells) following VPA treatment. Only the +29 vWF guide RNA was found to have enhanced cutting efficiency ($p = 0.0464$). However, an enhancement in cutting efficiency was evident in these cells following pretreatment with NaB. The cutting efficiency of the +23 ($p = 0.0061$), +29 ($p = 0.0287$), −36 ($p = 0.0086$) and the +39 ($p = 0.0369$) vWF guide RNAs were found to be increased in Jurkat cells (Fig. 3E). In addition, a similar though nonsignificant trend was observed with the −16 vWF guide RNA ($p = 0.1477$) (Fig. 3E).

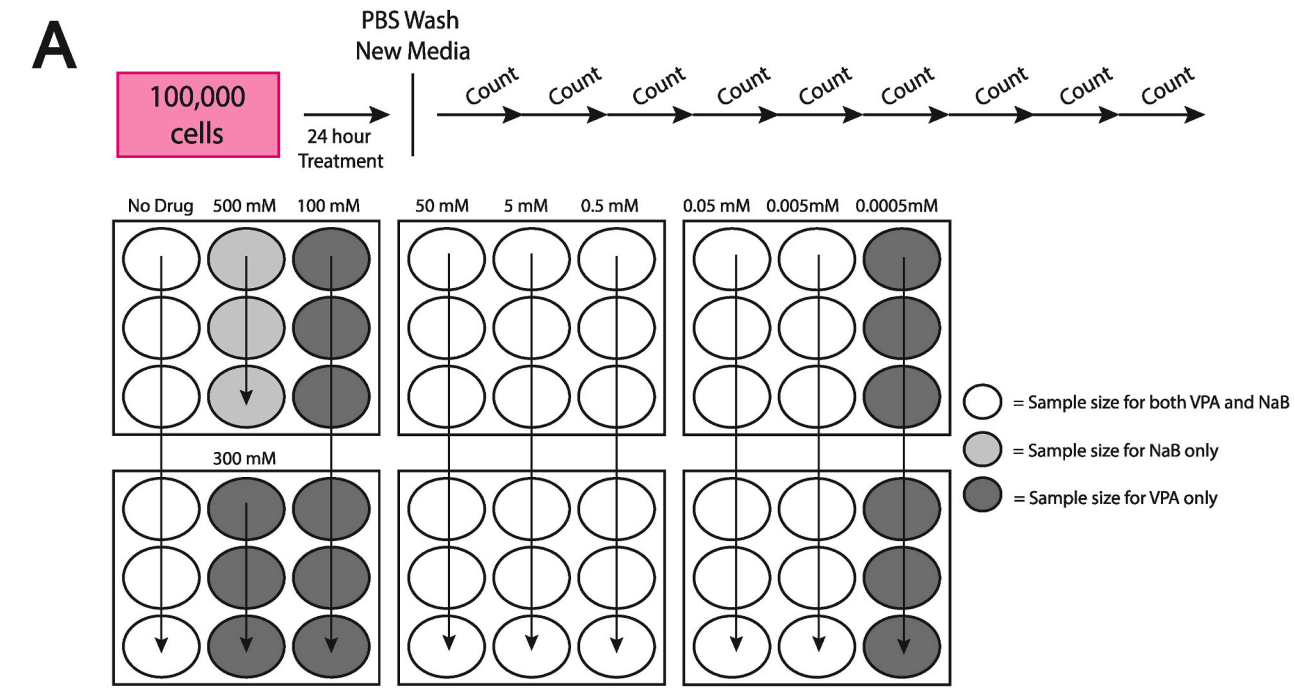

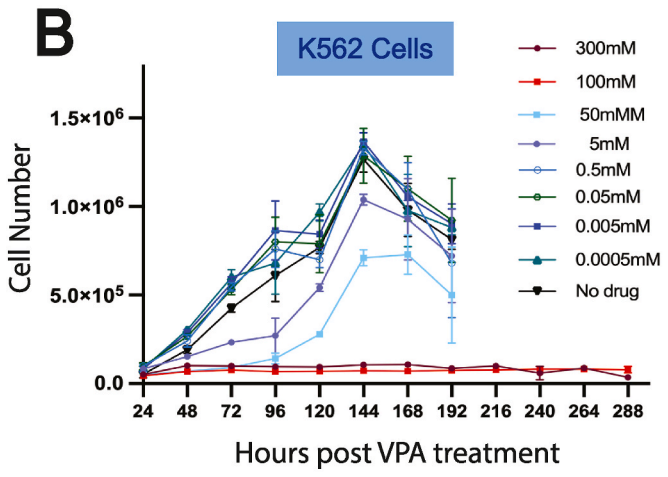

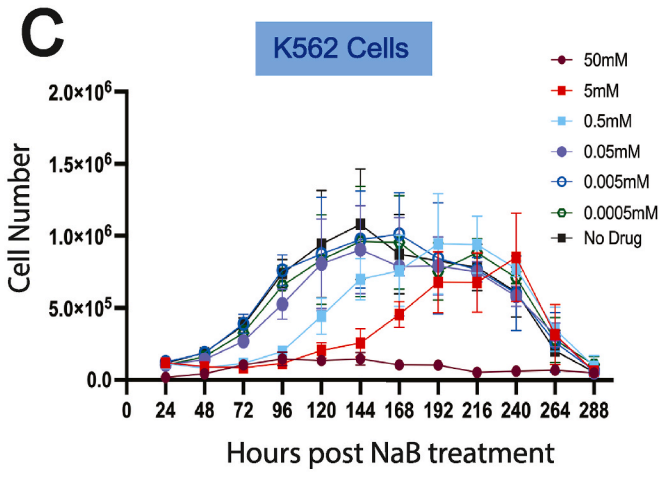

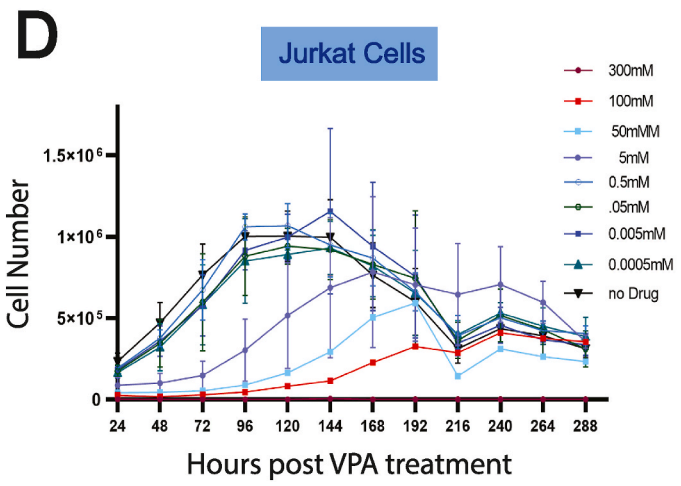

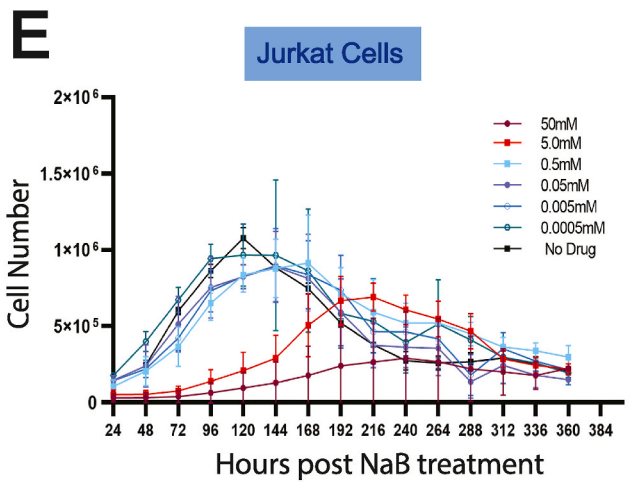

(caption on next page)

Fig. 1. Effect of VPA and NaB on the Growth Curve and Viability of K562 and Jurkat cells. A) Schematic representation of the experimental design. After treatment with either VPA or NaB for 24 h, the cells were washed and replated. Light gray wells were treated with only NaB (n = 3 for 500 mM), and dark gray wells were treated with only VPA (n = 3 for 300 mM, n = 6 for 100 mM). Unshaded wells indicate the sample sizes for both VPA and NaB-treated cells (n = 6 for each). B) K562 cell counts up to 11 days following VPA treatment. All conditions except for the 300 mM dose were performed with an n = 6. C) K562 cell counts up to 11 days following NaB treatment. All conditions except for the 500 mM dose were performed with an n = 6. D) Jurkat cell counts up to 11 days following VPA treatment. All conditions except for the 300 mM (n = 3) dose were performed with an n = 6. E) Jurkat cell counts up to 14 days following NaB treatment. All conditions were performed with an n = 6.

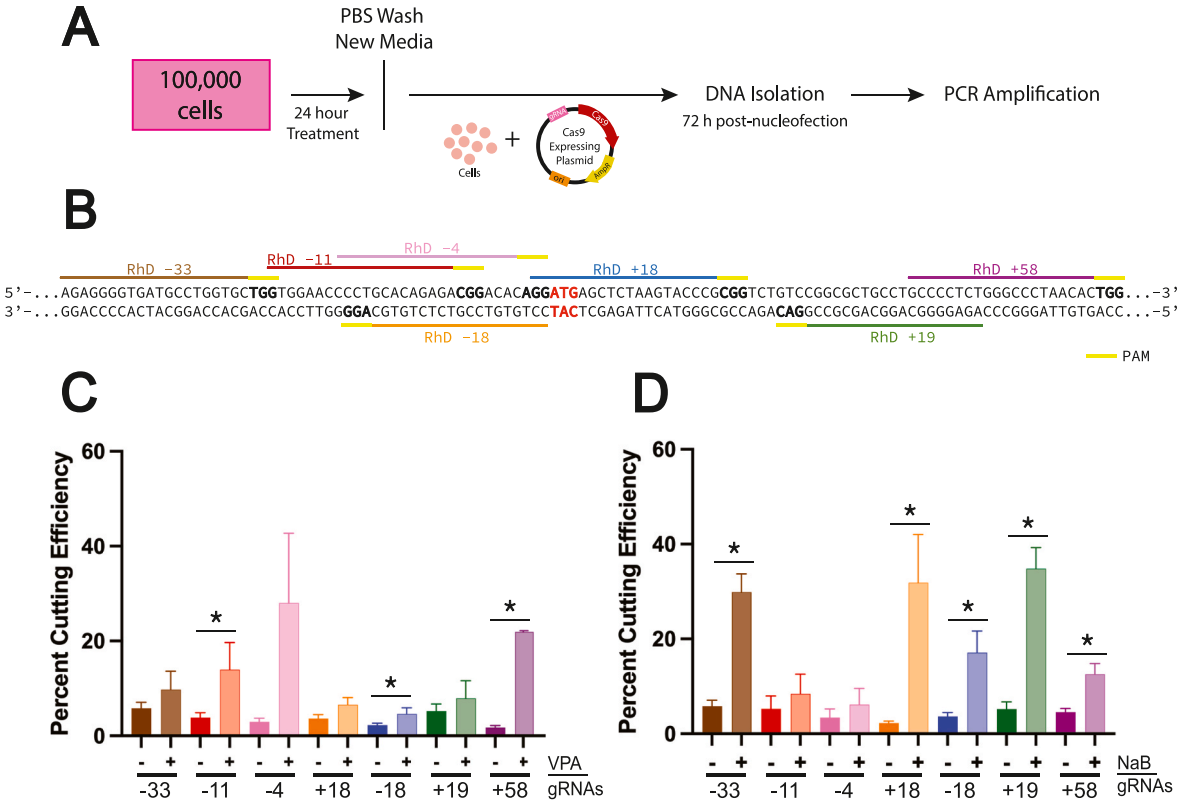

Fig. 2. Effect of VPA and NaB on the cutting efficiency of RhD CRISPR guide RNAs. A) Schematic of experimental design. B) Diagram of guide RNAs specific to the *RhD* locus used. Guide RNAs were named in reference to the *RhD* start codon ATG (bolded in red). The protospacer adjacent motif (PAM) (NGG for Cas9) for each guide RNA is identified by a yellow line and bolded. C) Cutting efficiency of the RhD guide RNAs with and without VPA or D) NaB pretreatment in K562 cells. The color of each bar correlates with the guide above. (For interpretation of the references to color in this figure legend, the reader is referred to the Web version of this article.)

3.4. HDACi enhance targeting efficiency

Based on the above observed increase in cutting efficiency of K562 cells at the *RhD* locus, the effect of HDACi on CRISPR/Cas9 editing was evaluated. We chose to evaluate the effectiveness of VPA solely as this compound is an FDA-approved pharmacological agent [17]. K562 cells were first treated with 0.005 mM of VPA (n = 10) for 24 h. After 24 h, both untreated (n = 10) and treated cells were nucleofected with a GFP containing donor DNA repair template and Cas9 expressing plasmid containing the most efficient RhD guide RNA. In this manner, a double-strand break could be corrected using the donor DNA repair template via the endogenous HDR pathway. As such, expression of GFP would be driven from the *RhD* promoter and could be used to visually identify successfully edited K562 cells. Following the 72-h incubation, GFP-positive K562 cells were quantified using flow cytometry. The number of GFP-positive cells was significantly increased as a result of VPA treatment, as high as 2-fold ($p < 0.0001$). Specifically, on average, there was a 1.6-fold increase in the amount of *RhD*-targeted cells pre-treated with VPA as compared to untreated cells (Fig. 4B). Targeting of the *RhD* locus was confirmed through PCR amplification (Fig. 4C) and subsequent sequencing (Fig. 4D). It is important to consider that the forward primer used annealed upstream of the homologous region found within the donor DNA repair template to ensure targeted integration as opposed to random integration.

4. Discussion

Nuclear DNA is wrapped around proteins known as histones. The acetylation of histones is managed by the interplay between histone acetyltransferases (HATs) and histone deacetylases (HDACs). HATs acetylate lysine residues on histone proteins yielding a relaxed chromatin structure. HDACs, on the other hand, are responsible for the DNA wrapping process and achieve this through the removal of an acetyl group from these histone proteins. In humans, there are 18 HDAC enzymes that fall into four classes: Class I proteins (HDACs 1–3 & 8), II proteins (HDACs 4–7, & 9), III proteins (SIRT1-7), and IV proteins (HDAC11) [18]. In the event of a condensed chromatin structure, the CRISPR/Cas9 enzyme is restricted from accessing genomic DNA, making it difficult to produce DSBs. Thus, HDACi can be used to enhance CRISPR/Cas9 cutting efficiency and furthermore enhance HDR-mediated repair when providing a repair DNA template in primary cell types.

HDACi are categorized as either short-chain fatty acids, hydroxamic acids, cyclic tetrapeptides, or benzamides [19]. Both VPA and NaB are

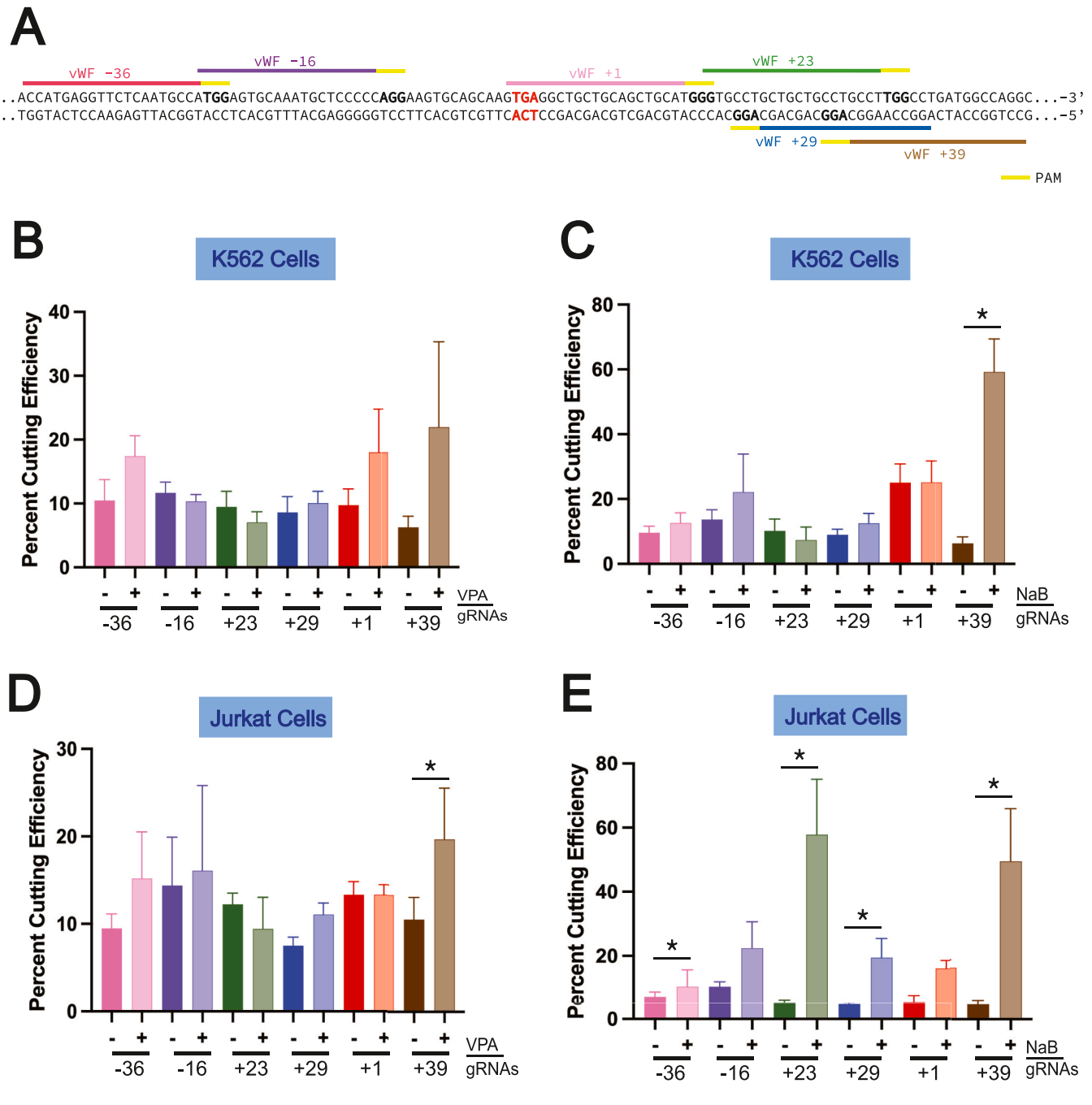

Fig. 3. Effect of VPA and NaB on the cutting efficiency of vWF CRISPR guide RNAs. A) Schematic diagram of guide RNAs specific to the *vWF* locus used. Guide RNAs were named in reference to the *vWF* stop codon TGA (bolded in red). The color of each guide correlates with the color of the bars below. B) Cutting efficiency of vWF guide RNAs in K562 cells with or without VPA pretreatment. C) Cutting efficiency of the vWF guide RNAs in K562 cells with or without NaB treatment. D) Cutting efficiency of vWF guide RNAs in Jurkat cells with or without VPA pretreatment. E) Cutting efficiency of the vWF guide RNAs in Jurkat cells with or without NaB treatment. (For interpretation of the references to color in this figure legend, the reader is referred to the Web version of this article.)

short-chain fatty acid HDACi. VPA, an established anti-epileptic drug, induces proteasomal degradation of HDAC2 and inhibits the catalytic activity of class I HDACs [20] while NaB has been shown to block both class I and class II HDACs [21]. We assessed the performance of these two specific HDACi in two blood cell lines. In regards to growth and viability, lower concentrations of each HDACi did not have an effect as compared to the no drug control in either cell line. Interestingly, the lymphoid representative Jurkat cell line was observed to be more sensitive to HDACi treatment than the myeloid representative K562 cell line. This difference in HDACi tolerance could be explained by increased genomic instability of the K562 cells [22,23]. While concentrations as high as 0.5 mM had little to no effect on growth or viability, we chose a conservative HDACi concentration of 0.005 mM for pretreatment in subsequent experiments to assess CRISPR/Cas9 cutting efficiency. This is noteworthy considering that concentrations as high as 1 mM VPA have been noted to induce differentiation of hematopoietic cell lines while concentrations as low as 0.2 mM VPA did not [24]. We note that it may be possible to observe even further enhancements in cutting efficiency if concentrations higher than 0.005 mM were to be used.

The effects of VPA and NaB on cutting efficiency of the RhD CRISPR

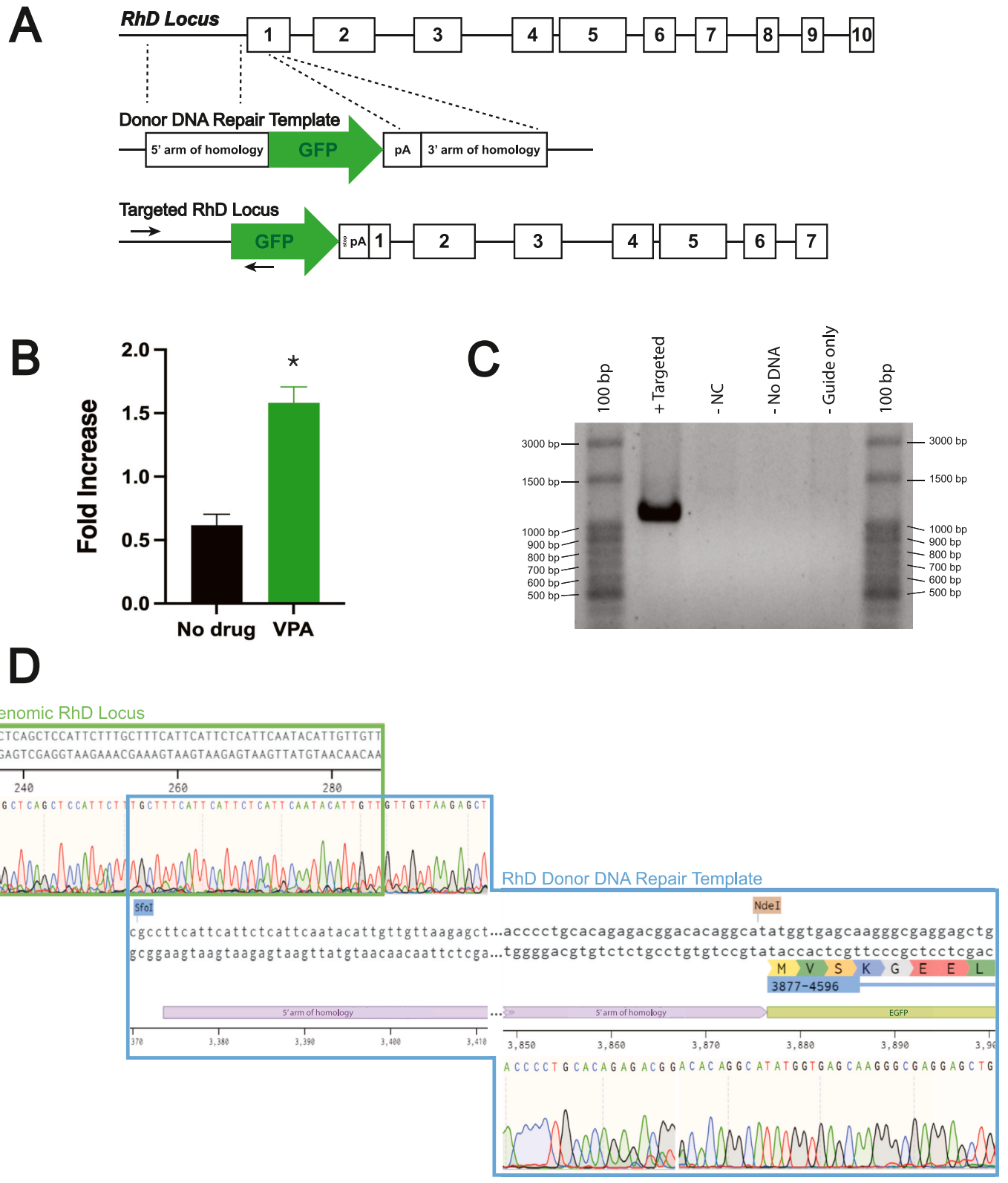

Fig. 4. Effect of VPA on CRISPR targeting efficiency of the *RhD* locus. A) Schematic depiction of targeting strategy. Primers used for subsequent analysis indicated by small black arrows. B) GFP-positive K562 cells indicative of gene targeting quantified via flow cytometry displayed as a fold change from baseline. C) PCR amplified of the region surrounding the targeting event (Targeted = electroporated with both the donor DNA repair template and guide RNA, NC = non-electroporated negative control; No DNA = electroporated without DNA additions; Guide only = electroporated without the donor DNA repair template). Successful integration of GFP is indicated by a band size of 1124bp. D) Sequencing of the PCR product indicated successful targeting of GFP to the *RhD* locus.

guide RNAs showed an overall upwards trend. Specifically, three RhD guide RNAs (−11, −18, and +58) yielded a statistically significant increase following VPA pretreatment (Fig. 2C). Of the seven guide RNAs tested following NaB treatment, five demonstrated an enhancement in cutting efficiency (−33, +18, −18 + 19, and +58) (Fig. 2D). The effect of HDACi on a second set of CRISPR guide RNAs, however, was not as evident. VPA did not have much of an effect on the vWF CRISPR guide RNAs in both K562 and Jurkat cells with only one guide (+29) having a significant enhancement in cutting efficiency. This suggests that the effect of VPA may be locus-specific. However, pretreatment with NaB was found to significantly enhance the cutting efficiency of four vWF guide RNAs (+23, +29, −36, and +39) in Jurkat cells and one guide RNA (+39) in K562 cells. It is possible that this is due to the extended ability of NaB to inhibit both class I and II histone deacetylases as opposed to VPA having an effect on only class I. Thus, NaB may be more beneficial for the enhancement of cutting efficiency than VPA. However, it is possible that an enhancement with this set of guide RNAs might be achieved with a VPA concentration higher than 0.005 mM.

With the use of a donor DNA repair template, a 1.6-fold increase in gene-edited cells was observed upon pre-treatment with VPA in K562 cells. It is important to note that HDACi, like VPA, can change the balance between the deacetylating activity of HDACs and the acetylating activity of HATs. This could lead to an increased histone acetylation and as a consequence an upregulation of gene expression [25]. However, it is unlikely that the enhancement we observed is due to an increase in expression alone as we have already demonstrated that pretreatment with an HDACi increases the amount of DSBs induced by Cas9 at the *RhD* locus. Thus, it is reasonable to conclude that the increase in GFP-positive cells observed is due to an enhancement in repair of the increased DSBs produced by the process of HDR.

CHSCs are historically difficult to edit using the CRISPR/Cas9 system. These experiments demonstrate that however small the enhancement, it is possible to increase CRISPR/Cas9 cutting efficiency and HDR in the further differentiated progenitor populations represented in this case by K562 and Jurkat cell lines. We remain optimistic that the use of HDACi will prove valuable to this field especially since the use of concentrations of HDACi greater than 0.005 mM may be found to further enhance cutting efficiencies and can easily be incorporated into essentially any CRISPR/Cas9 genome editing protocol.

Declaration of competing interest

The authors declare the following financial interests/personal relationships which may be considered as potential competing interests: Jennifer Johnston reports financial support was provided by National Institute of General Medical Sciences. Jennifer Johnston reports financial support was provided by California State University Program for Education and Research in Biotechnology. Guadalupe Castaneda reports financial support was provided by National Institute of General Medical Sciences. Codey Huang reports financial support was provided by California State University Program for Education and Research in Biotechnology.

Acknowledgements

This work was supported by the National Institutes of General Medical Sciences [5SC2GM126551, 4T34GM008253] and the CSU Program for Education and Research in Biotechnology.

Appendix A. Supplementary data

Supplementary data to this article can be found online at https://doi.org/10.1016/j.bbrep.2023.101513.

References

[1] P. Mali, L. Yang, K.M. Esvelt, J. Aach, M. Guell, J.E. DiCarlo, et al., RNA-guided human genome engineering via Cas9, Science 339 (6121) (2013) 823–826, https://doi.org/10.1126/science.1232033.
[2] F. González, Z. Zhu, Z.-D. Shi, K. Lelli, N. Verma, Q.V. Li, et al., An iCRISPR platform for rapid, multiplexable, and inducible genome editing in human pluripotent stem cells, Cell Stem Cell 15 (2) (2014) 215–226, https://doi.org/10.1016/j.stem.2014.05.018.
[3] P. Genovese, G. Schiroli, G. Escobar, T.D. Tomaso, C. Firrito, A. Calabria, et al., Targeted genome editing in human repopulating haematopoietic stem cells, Nature 510 (7504) (2014) 235–240, https://doi.org/10.1038/nature13420.
[4] M. Milyavsky, O.I. Gan, M. Trottier, M. Komosa, O. Tabach, F. Notta, et al., A distinctive DNA damage response in human hematopoietic stem cells reveals an apoptosis-independent role for p53 in self-renewal, Cell Stem Cell 7 (2) (2010) 186–197, https://doi.org/10.1016/j.stem.2010.05.016.
[5] J. Wang, C.M. Exline, J.J. DeClercq, G.N. Llewellyn, S.B. Hayward, P. Li, et al., Homology-driven genome editing in hematopoietic stem and progenitor cells using ZFN mRNA and AAV6 donors, Nat. Biotechnol. 33 (12) (2015) 1256–1263, https://doi.org/10.1038/nbt.3408.
[6] G. Li, X. Zhang, C. Zhong, J. Mo, R. Quan, J. Yang, et al., Small molecules enhance CRISPR/Cas9-mediated homology-directed genome editing in primary cells, Sci. Rep. 7 (8943) (2017), https://doi.org/10.1038/s41598-017-09306-x.
[7] M. Mohrin, E. Bourke, D. Alexander, M.R. Warr, K. Barry-Holson, M.M. Le Beau, et al., Hematopoietic stem cell quiescence promotes error-prone DNA repair and mutagenesis, Cell Stem Cell 7 (2) (2010) 174–185, https://doi.org/10.1016/j.stem.2010.06.014.
[8] V.T. Chu, T. Weber, B. Wefers, W. Wurst, S. Sander, K. Rajewsky, et al., Increasing the efficiency of homology-directed repair for CRISPR-Cas9-induced precise gene editing in mammalian cells, Nat. Biotechnol. 33 (5) (2015) 543–548, https://doi.org/10.1038/nbt.3198.
[9] C. Yu, Y. Liu, T. Ma, K. Liu, S. Xu, Y. Zhang, et al., Small molecules enhance CRISPR genome editing in pluripotent stem cells, Cell Stem Cell 16 (2) (2015) 142–147, https://doi.org/10.1016/j.stem.2015.01.003.
[10] T. Maruyama, S.K. Dougan, M. Truttmann, A.M. Bilate, J.R. Ingram, H.L. Ploegh, Inhibition of non-homologous end joining increases the efficiency of CRISPR/Cas9-mediated precise [TM: inserted] genome editing, Nat. Biotechnol. 33 (5) (2015) 538–542, https://doi.org/10.1038/nbt.3190.
[11] S. Riesenberg, T. Maricic, Targeting repair pathways with small molecules increases precise genome editing in pluripotent stem cells, Nat. Commun. 4 (9) (2018), https://doi.org/10.1038/s41467-018-04609-7, 2164.
[12] C.-Y. Gui, L. Ngo, W.S. Xu, V.M. Richon, P.A. Marks, Histone deacetylase (HDAC) inhibitor activation of p21WAF1 involves changes in promoter-associated proteins, including HDAC1, Proc. Natl. Acad. Sci. U. S. A. 101 (5) (2004) 1241–1246, https://doi.org/10.1073/pnas.0307708100.
[13] L. Cong, F.A. Ran, D. Cox, S. Lin, R. Barretto, N. Habib, et al., Multiplex genome engineering using CRISPR/cas systems, Science 339 (6121) (2013) 819–823, https://doi.org/10.1126/science.1231143.
[14] E.V. Brinkman, T. Chen, M. Amendola, B.V. Steensel, Easy quantitative assessment of genome editing by sequence trace decomposition, Nucleic Acids Res. 42 (22) (2014) e168, https://doi.org/10.1093/nar/gku936.
[15] M. Uhlen, P. Oksvold, L. Fagerberg, E. Lundberg, K. Jonasson, M. Forsberg, et al., Towards a knowledge-based human protein atlas, Nat. Biotechnol. 28 (2010) 1248–1250, https://doi.org/10.1038/nbt1210-1248.
[16] M. Uhlen, M. Karlsson, W. Zhong, A. Tebani, C. Pou, J. Mikes, et al., A genome-wide transcriptomic analysis of protein-coding genes in human blood cells, Science 366 (6472) (2019) 1–12, https://doi.org/10.1126/science.aax9198.
[17] H. Heers, J. Stanislaw, J. Harrelson, M.W. Lee, Valproic acid as an adjunctive therapeutic agent for the treatment of breast T cancer, Eur. J. Pharmacol. 835 (2018) 61–74, https://doi.org/10.1016/j.ejphar.2018.07.057.
[18] E. Seto, M. Yoshida, Erasers of histone acetylation: the histone deacetylase enzymes, Cold Spring Harbor Perspect. Biol. 6 (4) (2014) a018713, https://doi.org/10.1101/cshperspect.a018713.
[19] J. Biermann, J. Boyle, A. Pielen, W.A. Lagrèze, Histone deacetylase inhibitors sodium butyrate and valproic acid delay spontaneous cell death in purified rat retinal ganglion cells, Mol. Vis. 17 (2011) 395–403, 21311741.
[20] O.H. Krämer, P. Zhu, H.P. Ostendorff, M. Golebiewski, J. Tiefenbach, M.A. Peters, et al., The histone deacetylase inhibitor valproic acid selectively induces proteasomal degradation of HDAC2, EMBO J. 22 (13) (2003) 3411–3420, https://doi.org/10.1093/emboj/cdg315.
[21] M.J. Park, F. Sohrabji, The histone deacetylase inhibitor, sodium butyrate, exhibits neuroprotective effects for ischemic stroke in middle-aged female rats, J. Neuroinflammation 13 (1) (2016) 300, https://doi.org/10.1186/s12974-016-0765-6.
[22] L. Gioia, A. Siddique, S.R. Head, D.R. Salomon, A.I. Su, A genome-wide survey of mutations in the Jurkat cell line, BMC Genom. 19 (1) (2018) 334, https://doi.org/10.1186/s12864-018-4718-6.
[23] W. Parson, R. Kirchebner, R. Mühlmann, K. Renner, A. Kofler, S. Schmidt, et al., Cancer cell line identification by short tandem repeat profiling: power and

limitations, Faseb. J. 19 (3) (2005) 434–436, https://doi.org/10.1096/fj.04-3062fje.
[24] M. Göttlicher, S. Minucci, P. Zhu, O.H. Krämer, A. Schimpf, S. Giavara, J. P. Sleeman, F.L. Coco, C. Nervi, P.G. Pelicci, T. Heinzel, Valproic acid defines a novel class of HDAC inhibitors inducing differentiation of transformed cells, EMBO J. 20 (2001) 6969–6978, https://doi.org/10.1093/emboj/20.24.6969.
[25] H.P. Chen, Y.T. Zhao, T.C. Zhao, Histone deacetylases and mechanisms of regulation of gene expression (histone deacetylases in cancer), Crit. Rev. Oncog. 20 (2015) 35–47, https://doi.org/10.1615/critrevoncog.2015012997.